ACS OMEGA

Open Access

http://pubs.acs.org/journal/acsodf

Article

Glutamic Acid Enhances the Corrosion Inhibition of Polyaspartic Acid on Q235 Carbon Steel

Shichu Gong, Yutong Li, Hongyi Li, Lin He, Zhen Yan, Shuguang Wang, Xiaomin Sun, and Chao Song*

Cite This: *ACS Omega* 2023, 8, 39709−39719

Read Online

ACCESS | Metrics & More | Article Recommendations | Supporting Information

ABSTRACT: Currently, poly(aspartic acid) (PASP) is used with traditional toxic agents for corrosion inhibition, which greatly reduces the environmental significance of PASP as a green inhibitor. Amino acids, small-molecule compounds with amino and carboxyl groups, may react with PASP and act as chains to link PASP molecules, which might enhance the inhibition of PASP on metal corrosion. In this study, we selected glutamic acid (GLU) as a typical amino acid to explore the potential synergistic effect of the amino acid and PASP on corrosion inhibition via electrochemical experiments and molecular dynamics simulation. The corrosion inhibition of PASP was promoted by GLU with less weight loss and less pitting. The results of molecular dynamics simulation showed that GLU could bind with PASP at carboxyl groups and amino groups via donor−acceptor interactions and accelerate the diffusion of PASP to the carbon steel surface. Furthermore, the binding between PASP and the carbon steel surface can be enhanced by GLU, resulting in a dense and stable protective film. To the best of our knowledge, this is the first investigation into the mechanism of an amino acid as an enhancer to improve corrosion inhibition. This work provides a new strategy to enhance existing green inhibitors, which would significantly reduce the cost of cooling water treatment and its adverse environmental impacts.

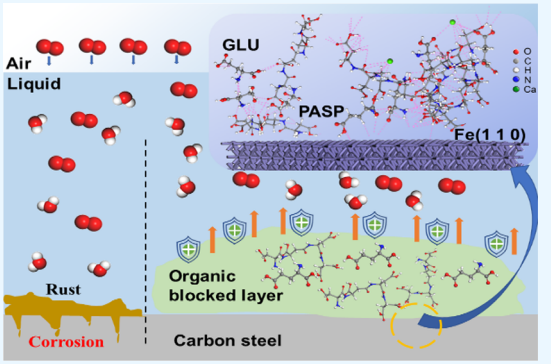

1. INTRODUCTION

Cooling water is widely applied in industries, including petroleum, electric, chemical, and metallurgical sectors.[1] To improve the heat transfer efficiency, thin walls are designed for heat exchanger tubes, and the thickness of fouling is strictly controlled. Once corrosion or fouling occurs in the heat exchanger, especially localized corrosion, the heat exchanger would quickly leak, causing significant production losses.[2−4] Therefore, it is vital to inhibit metal corrosion. Adding inhibitors is the most common method for corrosion inhibition due to its convenient operation and adjustability; i.e., the treatment dose can be adjusted depending on the water quality to ensure effective inhibition. Generally, inhibitors retard corrosion via forming a layer on the metal surface.[5] For example, heteroatomic compounds are the most common inhibitors because they have lone pairs of electrons in a p orbital, which could easily bond with the empty d orbitals of metals. However, most heterocyclic compounds, such as quinoline, pyridine, and indole, are nonbiodegradable and hazardous when released into the environment.[6−8] Therefore, it is necessary to develop novel inhibitors with a minimal negative environmental influence.

Polyaspartic acid (PASP), a polymeric amino acid that is rich in carboxylic acid side chains, is considered as a green inhibitor due to its excellent biodegradability by bacteria and fungi.[9] In a cooling water system, PASP could form a protective layer on the metal surface, block the active site, and weaken the anodic reaction.[10] Moreover, it can participate in nucleophilic reactions to form coordination bonds with the empty orbitals (d orbitals) on the metal surface, thus enhancing the stability of the chemisorbed layer on the metal surface.[11] However, it is difficult to achieve the desired effect when PASP is used alone, which reduces the environmental significance of using PASP as a green corrosion inhibitor.

Amino acids, abundant in nature, have been frequently studied as potential corrosion inhibitors.[12−14] The anticorrosion behavior of amino acids is mainly attributed to their amino and carboxyl groups.[15,16] It is worth noting that these special configurations may also interact with $-NH_2$ and −COOH in other amino acids and their derivatives, such as PASP.[17] Thus, it is reasonable to speculate that amino acids could react with PASP acting as chains to link PASP molecules, which might enhance corrosion inhibition by forming a denser film on the metal surface. However, the synergistic effect and mechanism of amino acid and PASP on corrosion inhibition

Received: August 1, 2023
Accepted: September 26, 2023
Published: October 10, 2023

are still not clear. In this study, glutamic acid (GLU) was selected as a representative amino acid to investigate its role in improving the corrosion inhibition of PASP for carbon steel. This study aims to (1) explore the corrosion of Q235 steel in the combination of PASP and GLU via morphologic analysis and electrochemical measurement and (2) reveal the synergistic mechanism of PASP and GLU on corrosion inhibition using molecular dynamics simulation.

2. EXPERIMENTS/METHODS

2.1. Chemicals and Materials. Polyaspartic acid (MW 7000, PASP >95%, solubility 15 g/100 mL at 25 °C) and glutamic acid (GLU, >98%, solubility 0.75 g/100 mL at 20 °C) were purchased from Shanghai Macklin Biochemical Co., Ltd. (Shanghai, China). Other chemicals were of analytical grade from Sinopharm Chemical Retreatment Corporation (China) and used without further purification. The Q235 carbon steel coupons were prepared with grinding, and their chemical composition was 0.22 C, 0.3 Si, 1.4 Mn, 0.01 Cr, 0.01 Ni, 0.045 P, 0.05 S, and Fe balance (wt %). All coupons were pretreated before use (Text S1). The simulated cooling water was composed of 0.735 g/L $CaCl_2{\cdot}2H_2O$, 0.658 g/L NaCl, 0.493 g/L $MgSO_4$, and 0.168 g/L $NaHCO_3$. The solution pH was adjusted to 8.0 ± 0.1 with a 1 M NaOH and 1 M HCl solution. Three experimental groups were tested in simulated cooling water: the labeled GLU group, PASP group, and PASP + GLU group. The concentrations of GLU and PASP were set at 10 and 40 mg/L, respectively. Blank groups were also prepared without GLU and PASP.

2.2. Weight Loss and Coupon Surface Analysis. The corrosion inhibition was first investigated with the rotating hanging piece method.[18,19] Briefly, three coupons in each group were immersed in simulated cooling water at 70 rpm and 35 ± 1 °C for 72 h. Then, all coupons were collected and cleaned with 2.4 M HCl, 1.5 M NaOH, and ethanol to remove the corrosion products on the surface. Finally, the coupons were weighed with an analytical balance. The corrosion rate (ν) and corrosion inhibition efficiency (η) were calculated according to the equations

$$\nu = \frac{8760 \times (m_1 - m_0) \times 10}{s \cdot \rho \cdot t} \quad (1)$$

$$\eta = \frac{\nu_0 - \nu_1}{\nu_0} \times 100\% \quad (2)$$

where m_0 and m_1 are the initial and final weight of the coupons, respectively (g), s is the coupon surface area (cm^2), t is the immersion time (h), ρ is the density of the coupon (g/cm^3), and ν_0 and ν_1 are the corrosion rates in the blank group and other groups, respectively.

The cleaned coupons were also observed using a scanning emission microscope (SEM, Quanta 250 FEG, USA) and an atomic force microscope (AFM, NanoWizard 4, GER). Roughness parameters, Ra and Rz, were measured with AFM to determine the average roughness and the average of the vertical distances between the highest ridges, respectively. Details are described in Text S2. The composition and elemental status of coupons were analyzed with XPS, which was performed with a Thermo Scientific K-Alpha instrument using a monochromatic Al Kα X-ray source ($h\nu$ = 1486.6 eV) at a residual pressure below 5.0×10^{-7} bar. Contact angles were measured with a contact angle meter (HSRKE-SPCA, China) to evaluate the surface hydrophobicity of coupons. All measurements were conducted at least three times at room temperature.

2.3. Electrochemical Measurement. The open circuit potential (OCP), electrochemical impedance spectrum (EIS), and potentiodynamic polarization curves (PDP) were analyzed using an electrochemical workstation (CHI 660e, CH Instruments Inc., USA). Before the measurement, the coupons were embedded in epoxy resin with an exposed area of 1 cm^2 as a working electrode. Electrochemical measurements were conducted in a three-electrode reactor, which is a glass vessel with a multichannel polytetrafluoroethylene cover. An Ag/AgCl (saturated KCl) electrode and graphite were used as reference and counter electrodes, respectively. EIS analysis was carried out at OCP using an amplitude sinusoidal signal of 10 mV with a frequency range from 1×10^5 to 1×10^{-2} Hz. The data were fitted with ZSimpWin software. The scanning range of PDP was based on the OCP value at ±0.3 V with a scan rate of 0.167 mv/s. All measurements were conducted at 35 ± 1 °C. The corrosion inhibition was calculated with the equation[20]

$$P_{corr},\ \% = \frac{I^0_{corr} - I^{inhibitor}_{corr}}{I^0_{corr}} \times 100\% \quad (3)$$

where I^0_{corr} and $I^{inhibitor}_{corr}$ are the corrosion currents in the blank group and experimental groups, respectively. The experiments were repeated at least three times to guarantee the experiment's repeatability.

2.4. Molecular Dynamics Simulation. To investigate the interaction of GLU and PASP on the iron substrate, molecular dynamics (MD) simulation was applied with the Forcite module in the Materials Studio 2018 software based on DFT theory.[21,22] The frontier orbital theory holds that there are "valence electrons" similar to a single atom in a molecule, and the valence electrons of a molecule are frontier electrons. Two molecular orbitals (MOs) in each molecule were calculated: the lowest unoccupied (LUMO) and highest unoccupied molecular orbitals (HOMO). The eigenvalues of LUMO and HOMO were represented by E_{LUMO} and E_{HOMO}, respectively. $E_{LUMO\text{-}HOMO}$ ($E_{L\text{-}H}$) was the eigenvalue difference between LUMO and HOMO. The fractions of exchanged electrons between carbon steel, PASP, and GLU were determined with the mentioned eigenvalues.[23−25]

The Fe (110) plane, as the most stable representative, was cleaved from a pure Fe crystal and then converted to a supercell with three layers of Fe (110). The calculations were applied using the COMPASSII force field at 308 K to optimize the chemical structures in all groups.[26] The Fe (110) surface, composed of three layers of Fe atoms, was built in a rhombic simulation box (x = 90.00 Å, y = 90.00 Å, and z = 70.53 Å). Then, three MD simulation models, containing organic molecules (GLU, PASP, and GLU + PASP), were built in an aqueous solution with ions (Mg^{2+}, HCO_3^-, Ca^{2+}, Na^+, SO_4^{2-}, and Cl^-), and were placed on the Fe (110) surface. The initial mole ratio of each polymer in the simulation models is in strict similarity to our experimental data. Finally, the three models were constructed in the same cubic simulation lattice. After potential overlaps among all molecules were removed by energy minimization, these three models were run to obtain an equilibrium state at a constant temperature and pressure with an optimized periodic boundary cell. Periodic boundary conditions were applied in the three models.

https://doi.org/10.1021/acsomega.3c05625
ACS Omega 2023, 8, 39709−39719

The long-range electrostatic interactions were analyzed with the Ewald method. The total energy is composed of diagonal and off-diagonal cross-coupling terms and nonbond interaction terms, which include the Coulombic and Lennard−Jones functions for electrostatic and van der Waals interactions[27,28]

$$E = E_{\text{bonds}} + E_{\text{angles}} + E_{\text{dihedrals}} + E_{\text{cross}} + E_{\text{VDW}} + E_{\text{elec}} \quad (4)$$

$$E_{\text{non-bond}} = E_{\text{VDW}} + E_{\text{elec}} = \sum \epsilon_{ij}\left[2\left(\frac{\sigma_{ij}}{r_{ij}}\right)^9 - 3\left(\frac{\sigma_{ij}}{r_{ij}}\right)^6\right] + \sum \frac{q_i q_j}{r_{ij}} \quad (5)$$

The parameters for each like-site interaction were calculated with the COMPASSII force field.[27,29] The energies of the initial configurations were minimized with the Smart Minimizer method. After minimization, all simulations were equilibrated at a constant temperature and volume for about 10 ns. Atomic coordinates were saved at every 500 ps. The analysis was performed by averaging the final 1 ns of each trajectory.

2.5. Statistical Analysis. Weight loss experiments and electrochemical measurements were conducted at least thrice, and three sets of parallel samples were set in each experiment. The error bars in the figures represent the standard deviation between the replicates. The data were analyzed with an independent t test standard deviation, and the significance levels were expressed at $^*p < 0.05$ and $^{**}p < 0.01$.

3. RESULTS AND DISCUSSION

3.1. Weight Loss and Surface Analysis. The weight loss of coupons was measured to evaluate the corrosion inhibition of PASP by the rotation specimen method. Figure 1A shows the average corrosion rate (ν) and corrosion inhibition efficiency (η) at different PASP concentrations for carbon steel in simulated cooling water, which were calculated from the weight loss. The inhibition increased at first and then decreased with increasing PASP concentration. The maximum ν was observed with 40 mg/L PASP, up to 44.3 ± 3.0%. This result could be explained by the role of organic ions in corrosion. It has been reported that PASP formed a protective layer on carbon steel to inhibit corrosion while organic ions from PASP were also an important factor that accelerates corrosion.[30] Therefore, corrosion inhibition decreased in the presence of high-concentration PASP due to the increasing amounts of organic ions. In this study, PASP at 40 mg/L was selected for subsequent experiments due to its excellent corrosion inhibition. As shown in Figure 1B, the carbon steels in the blank group corroded rapidly in simulated cooling water at 0.40 ± 0.049 mm/a. The corrosion rates were 0.34 ± 0.011 and 0.22 ± 0.012 mm/a in the presence of GLU and PASP, respectively. However, the PASP + GLU group showed the highest η of up to 53.7 ± 2.6%, suggesting that PASP and GLU exhibited intermolecular synergistic inhibition on corrosion. The existence of synergistic interaction between PASP and GLU on the carbon steel surface is quantified with the synergistic parameter (S) based on the η value. The value of S is calculated with the equations[31]

$$S = \frac{1 - \eta_{\%}^{\text{threshold}}}{1 - \eta_{\%}^{\text{measured}}} \quad (6)$$

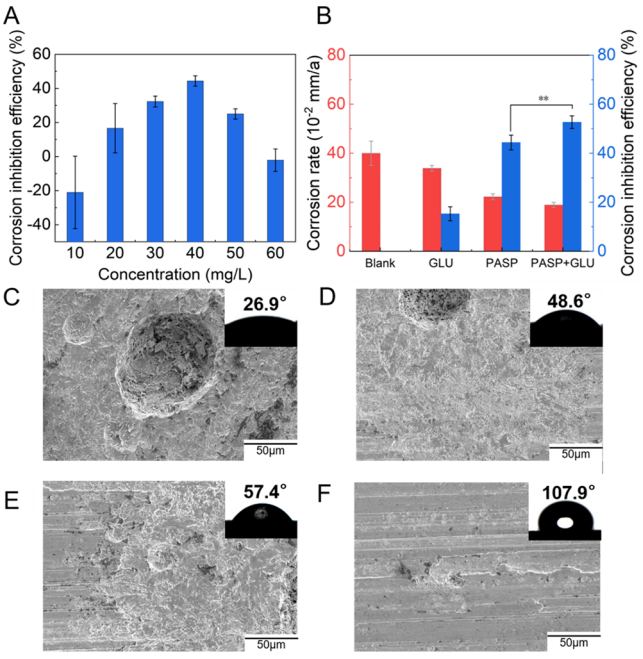

Figure 1. (A) Corrosion inhibition of carbon steel with different PASP concentrations. (B) Corrosion rate and corrosion inhibition rate in different groups. SEM images and contact angles of the coupons in Blank (C), GLU (D), PASP (E), and PASP + GLU groups (F). The concentrations of GLU and PASP were set at 10 and 40 mg/L, respectively. All coupons in each group were immersed in simulated cooling water at 70 rpm and 35 ± 1 °C for 72 h. Corrosion inhibition rates were calculated according to the corrosion of coupons in the blank group.

$$\eta_{\text{Aramaki}}^{\text{threshold}} = \eta_1 + \eta_2 - \eta_1\eta_2 \quad (7)$$

where $\eta^{\text{threshold}}$ is the threshold inhibition efficiency and η^{measured} is the measured inhibition efficiency. η_1, η_2, and $\eta_1\eta_2$ are the measured corrosion inhibition efficiencies of PASP, GLU, and the binary mixture, respectively. The interaction between PASP and GLU was synergistic, as indicated by the value of 1.14 ($S > 1$), and the calculation is shown in the Supporting Information. These results indicated that GLU enhances the role of PASP in corrosion inhibition.

The morphology of coupons was observed with SEM (Figure 1C−F). Rough surfaces and large pits were found on the coupon in the blank group, whereas surface corrosion was reduced with a smoother surface and less pitting in both the GLU group and PASP group. No obvious damage was observed in the PASP + GLU group, indicating that the combination of PASP and GLU could inhibit pitting corrosion on the coupons. These results were consistent with the weight loss measurements. Contact angle analysis and AFM were used to confirm that a protective layer is formed by PASP. The coupon surface in the blank group exhibited hydrophilicity with a contact angle of 26.9°, and more hydrophobic surfaces were detected in the presence of PASP with a contact angle of 57.4° in the PASP group and 107.9° in the PASP + GLU group. These results indicated that PASP formed a protective layer on the coupon surface, which was enhanced by GLU. A hydrophobic surface could retard the adhesion of corrosive substances on the surface, which also benefits corrosion inhibition.[32] Furthermore, the surface roughness of coupons was analyzed with AFM. As shown in Figure 2, the coupon surface was seriously corroded with Ra at 122.3 nm and Rz at

https://doi.org/10.1021/acsomega.3c05625
ACS Omega 2023, 8, 39709−39719

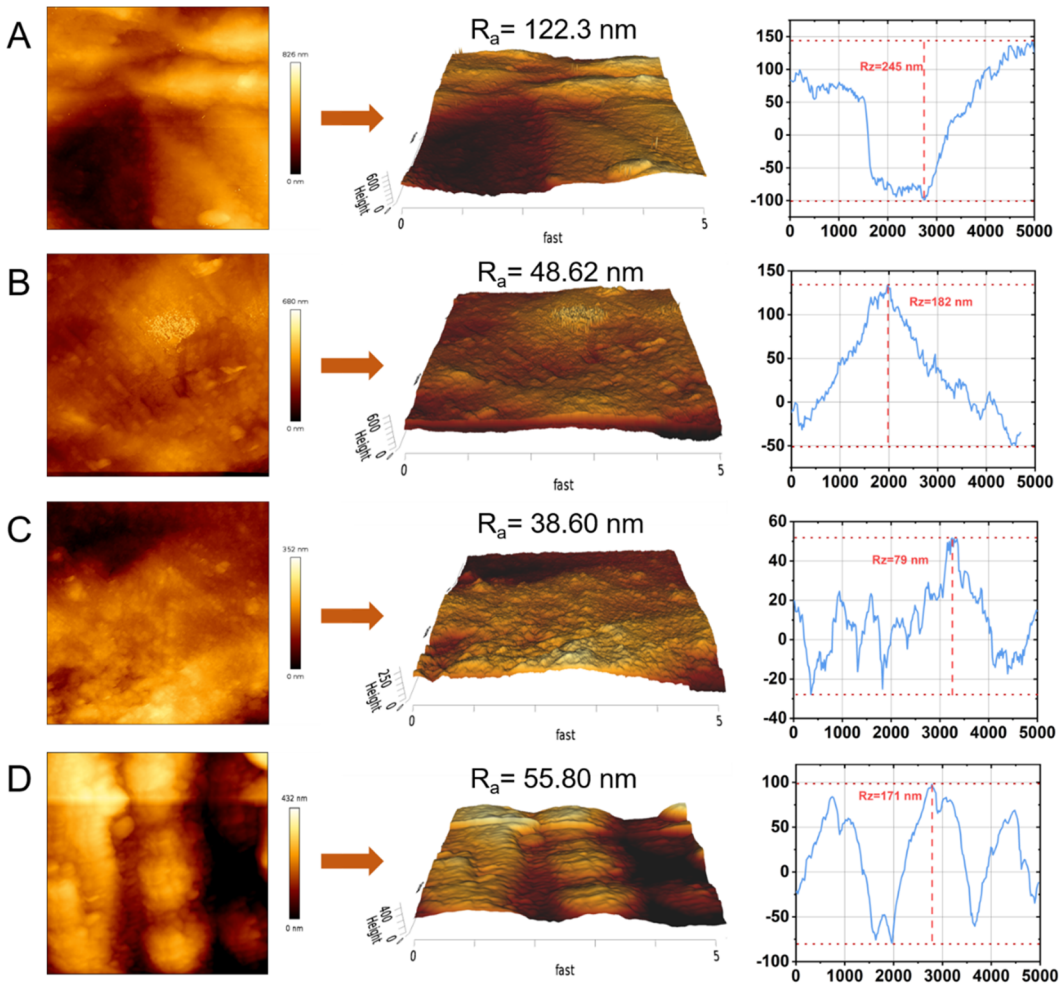

Figure 2. AFM images of carbon steel coupons after immersion for 72 h in Blank (A), GLU (B), PASP (C) and PASP + GLU groups (D).

245 nm in the blank group due to direct contact with cooling water. The addition of PASP and GLU reduced the surface roughness of coupons in the GLU group (Ra = 48.62 nm, Rz = 182 nm), PASP group (Ra = 38.60 nm, Rz = 79 nm), and PASP + GLU group (Ra = 55.80 nm, Rz = 171 nm), confirming the formation of a protective layer by PASP and GLU on the coupon surface. Besides, scratches due to grinding were observed in the PASP + GLU group (Figure 2D), which could explain why the coupon exhibited higher roughness than that in the PASP group.

XPS was applied to further evaluate the corrosion of the coupons (Figure 3). For C 1s, the three peaks at 284.8, 285.4, and 290.8 eV correspond to C−C, C−O−R, and C═O, respectively. Besides, there are COOR and C−N in the case with PASP + GLU. For the O 1s spectrum, three binding energies are identified at 529.4 eV (O−M), 532.5 eV (C═O), and 532 eV (C−O and O−H). For the N 1s spectrum, one peak is present at 398.6 eV, which belongs to C−NH−.[33] For the Fe 2p spectrum, there are two peaks at 711.7 and 710.1 eV, corresponding to Fe(II) (such as FeO, $FeCO_3$) and Fe(III) (such as Fe_2O_3, FeOOH), respectively, where for the sample with PASP + GLU, there was only the metallic Fe peak (707.6 eV).[34]

3.2. EIS and PDP Analysis. The anticorrosion effect was investigated with EIS tests. As shown in Figure 4, Nyquist and Bode plots were recorded at different immersion times. In all groups, the Nyquist plots exhibited an extended capacitive loop. Then, impedance analysis, such as fitting to the appropriate circuit, was performed to determine the number of semicircles. The capacitive loop actually consisted of two capacitive semicircles with similar time constants according to the χ^2 value in Table S1. Therefore, an equivalent model with two time constants was employed to account for both layer formation and charge transfer. Based on these, an equivalent circuit was designed to fit EIS data (Figure 5A and Table S1). In this model, Q is the constant phase element (CPE), which is associated with surface roughness and an oxide passive layer in the medium and low-frequency.[35] R_s, R_f, and R_{ct} indicate the resistances of the electrolyte, surface layer, and electrical double layer, respectively. R_{ct} reflects the passive layer or corrosion products formed on the surface of the coupons.[36] A high R_{ct} value implies strong corrosion inhibition.[35] The value of n is in the range of 0.52−0.93, suggesting the inhomogeneity of the steel surface after corrosion in the solution with or without inhibitors and the corrosion of carbon steel in the solution being primarily controlled by the charge transfer.

In this study, much higher R_{ct} values were obtained at 2 and 3 d in the PASP + GLU group than those in the PASP group, confirming the role of GLU in improving the corrosion inhibition of PASP. Moreover, R_{ct} values decreased rapidly at 4 and 5 d due to the breach of a protective layer, which was consistent with the Nyquist plots. After a 1-day immersion, the

https://doi.org/10.1021/acsomega.3c05625
ACS Omega 2023, 8, 39709−39719

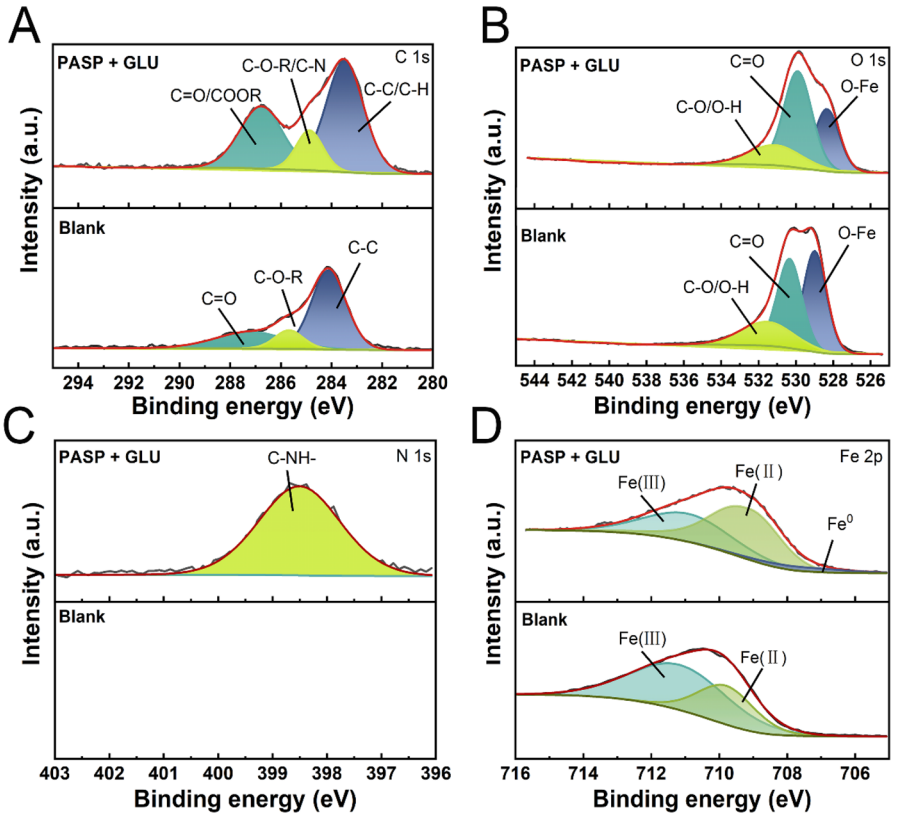

Figure 3. High-resolution XPS of coupons in Blank and PASP+GLU groups after immersion at 35 ± 1 °C for 72 h: (A) C 1s, (B) O 1s, (C) N 1s, and (D) Fe 2p.

radii of capacitive loops in the PASP + GLU group were much larger than those in other groups, suggesting the improved corrosion inhibition in the presence of PASP + GLU.[37] The radii reached their maximum at 3 d and then decreased at 4 and 5 d, which was attributed to the breach of the protective layer.[38] It is worth noting that a smaller radius was detected in the PASP + GLU group than that in the PASP group at 2 h, indicating that less PASP was attached to the coupon surface in the presence of GLU. This might be due to GLU hindering the ballistic motion of PASP and thus retarding the movement of PASP to the coupon surface at the beginning.

Potentiodynamic polarization curves of Q235 carbon steel were also employed to assess the corrosion of coupons. As shown in Figure 6, the shape of the polarization curve in the PASP + GLU group was significantly different from that in the blank group, indicating distinct kinetics for both the anode and cathode reactions. The change in the electron transfer may be attributed to the alteration of the protective film on the coupon surface. Additionally, metals with lower corrosion voltages exhibited higher corrosion rates, and a high corrosion potential was detected in the PASP+GLU group, suggesting the superior corrosion resistance of the coupons. Furthermore, the current density increased as the applied potential increased, indicating that the corrosion of carbon steel undergoes an activation-controlled process. Both the anodic and cathodic branches in the PASP + GLU group shift to a low current density direction compared with that in other groups, indicating that the presence of PASP + GLU inhibits both anodic and cathodic reactions at the same time, which is the mix-type corrosion inhibition mechanism. Extrapolation of the anodic and cathodic Tafel line was used to calculate i_{corr} (Table S2). i_{corr} in the PASP + GLU group was much lower than that in other groups (Figure 5B), indicating less corrosion occurred in the presence of both PASP and GLU. These results confirmed that the combination of PASP and GLU exhibited a better corrosion inhibition on carbon steel.

3.3. Molecular Dynamics Simulation. The interactions of PASP and GLU on the Fe (110) surface were simulated with DFT theory to explore the roles of PASP and GLU in corrosion inhibition. Generally, the dissociation and equilibrium of PASP are complicated in an aqueous solution, and thus, it is difficult to evaluate its coordination chemical behavior. However, the H_4L model was applied to simulate the PASP molecule for DFT calculation, which was used with high accuracy in previous studies.[39] Therefore, we selected the H_4L model in this study to investigate the behavior of PASP on the iron surface (Figure S1). The electronic properties of PASP and GLU molecules were extracted via ab initio DFT calculations, and the interaction-related electronics were derived using molecular orbital (MO) theory. Two MOs (HOMO and LUMO) intensely influence the interactive sites participating in a surface interaction via a donor−acceptor mechanism.[40−43] The HOMO works as an electron donor while the LUMO reflects a stronger affinity for electrons as an electron acceptor, and these two orbitals are those that interact most easily.[44] In this study, the favorable regions for HOMO of both GLU and PASP molecules were carboxyl groups (Figure 7B,E), suggesting that they might act as electron donors for potential acceptors such as metallic cations. The LUMO was mainly distributed in the amino groups and adjacent carbon chains in both molecules (Figure 7C,F). Therefore, GLU and PASP molecules may bind with each other via donor−acceptor interactions between carboxyl groups and amino groups.

https://doi.org/10.1021/acsomega.3c05625
ACS Omega 2023, 8, 39709−39719

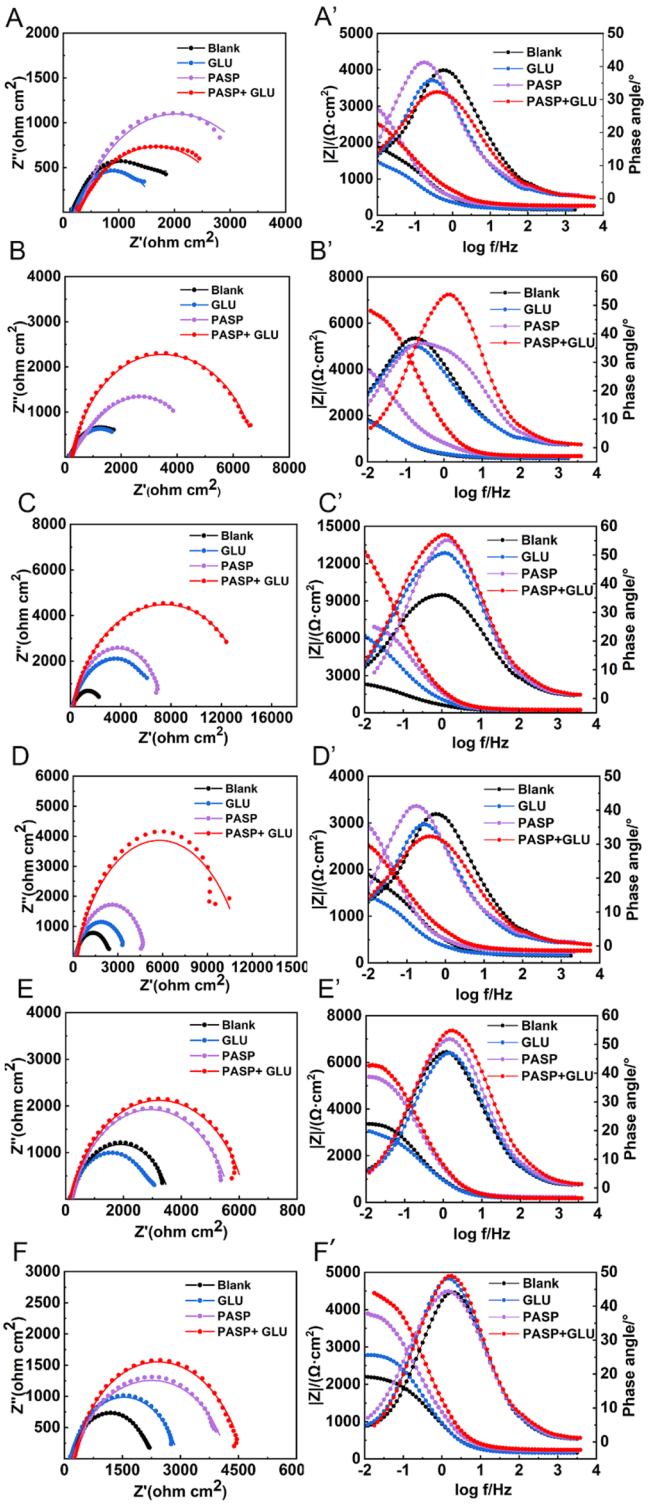

Figure 4. Nyquist and Bode plots of carbon steel in different groups at 2 h (A, A′), 1 d (B, B′), 2 d (C, C′), 3 d (D, D′), 4 d (E, E′), and 5 d (F, F′).

The bonding interaction between inhibitors and the Fe surface is dependent upon the energetic positions of PASP, GLU, and PASP + GLU (E_{HOMO}, E_{LUMO}). In Table 1, E_{HOMO} and E_{LUMO} represent the ability of inhibitor molecules to provide electrons to empty metal orbitals and accept electrons, respectively. For PASP and PASP + GLU, a higher E_{HOMO} of PASP + GLU suggests that the electrons could be excited from the HOMOs of PASP + GLU to the Fe surface. PASP + GLU exhibited a higher E_{HOMO} and lower E_{LUMO} than PASP, suggesting that the electrons could be excited from the HOMOs of PASP + GLU to the Fe surface.[23] Moreover, the ΔE value (3.423 eV) of PASP + GLU is smaller than that of PASP (3.725 eV). This indicates that there is easier electron transfer between PASP + GLU and the Fe surface.[45,46] Intermolecular forces, such as hydrogen bond force and van der Waals force, were calculated with MD simulation to explore the interaction between the PASP and GLU molecules. As shown in Figure 7G, hydroxyl and amino groups in the GLU molecule could bind with carboxyl groups in the PASP molecule via van der Waals forces. The binding between the occupied orbital of GLU and the unoccupied orbital of PASP results in mutual attraction, confirming the interaction between GLU and PASP.[40] These results were consistent with the MO calculation results.

3.4. Mean Square Displacements. The diffusion coefficients of PASP and GLU molecules were also calculated by directly measuring the mean square displacement (MSD) of the mass center of the targets from the MD trajectory to evaluate their movement in simulated cooling water. The MSD of the two target molecules was obtained from the equation

$$\mathrm{MSD}(t) = \left\langle \frac{1}{N}\sum_{i=1}^{N} |r_i(t) - r_i(0)|^2 \right\rangle \tag{8}$$

where N is the number of target molecules and $r_i(t)$ is the position of molecule i at time t. The diffusion coefficient represents the mobility of molecules and mainly depends on the MSD behavior. To compute the diffusivity properly, the diffusing entity must escape its solvation shell several times. Typically, an ionic entity with hysteresis dynamics describes three types of diffusion regions based on its calculated MSDs. In this study, at the initial time (0−40 ps), the free motion of PASP appeared as a more intense ballistic motion. In the intermediate time (40−700 ps), the ion motion reached the subdiffusive regions, where the MSD values in PASP + GLU group exceeded those in the GLU group and PASP group, indicating that these molecules' mobility intensify. Subsequently, the system dynamics of PASP are usually regulated by random collisions with the nearest neighboring species (GLU) and exhibit extremely high MSD values. Moreover, the MSD curves of both GLU and PASP in the PASP + GLU group were linear, and the values increased with time (Figure 8A). The slopes of the MSD curves in the PASP + GLU group were significantly higher than those in other two groups, implying that the diffusion of PASP was greatly improved by GLU. The diffusion coefficients (D_α) were obtained from the slope of the mean square displacement versus the time curve, using the well-known Einstein relation

$$D_\alpha = \frac{1}{6N_\alpha}\lim_{t\to\infty}\frac{\mathrm{d}}{\mathrm{d}t}\sum_{i=1}^{N_\alpha}\langle [r_i(t) - r_i(0)]^2\rangle \tag{9}$$

where d is the dimensionality of the model and $r_i(t)$ and $r_i(0)$ are the center-of-mass coordinates of the ith target molecule at times t and 0, respectively. As shown in Figure 8B, D_α values of GLU and PASP were quite low when they existed alone in the GLU group and PASP group, respectively. However, the values increased significantly in the PASP + GLU group, suggesting the stronger diffusion ability of GLU and PASP when they both were present. These results confirmed that GLU could

https://doi.org/10.1021/acsomega.3c05625
ACS Omega 2023, 8, 39709−39719

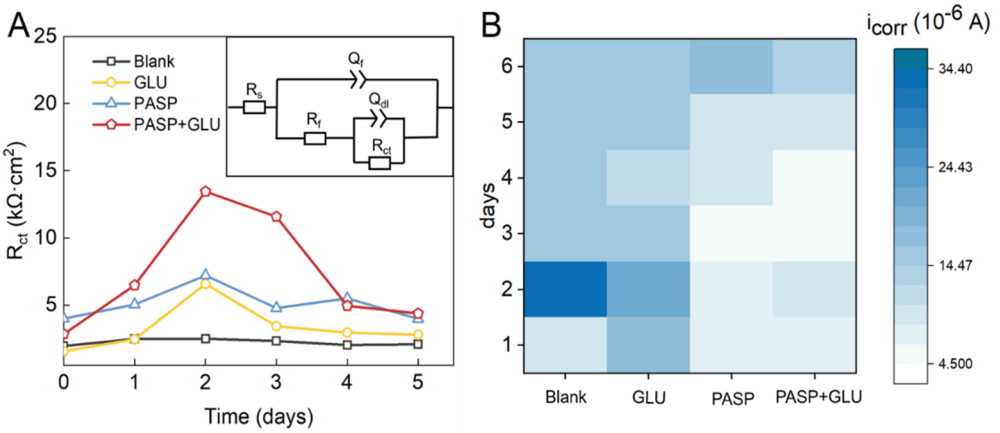

Figure 5. Equivalent circuit (insert) and R_{ct} values in different groups (A). i_{corr} values of each group (B).

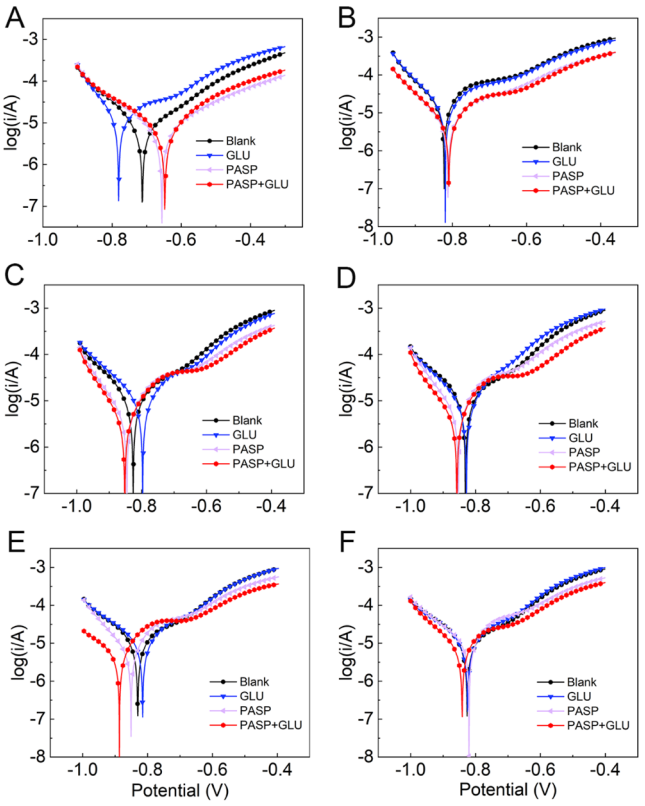

Figure 6. Potentiodynamic polarization curves of carbon steel in different groups at 2 h (A), 1 d (B), 2 d (C), 3 d (D), 4 d (E), and 5 d (F).

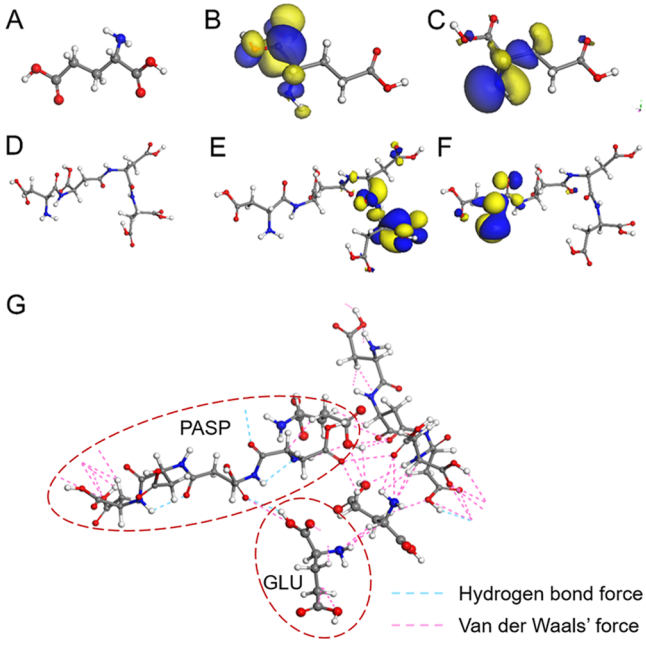

Figure 7. Optimized molecular structure models of GLU (A) and PASP (D) for MD simulation. LUMO (B, E) and HOMO (C, F) frontier orbitals of PASP (the blue and yellow colors represent the positive and negative phases of the molecular orbitals, respectively). Interaction between PASP and GLU obtained by molecular simulation (G).

enhance the diffusion of PASP on carbon steel surfaces, which favors corrosion inhibition.

3.5. Binding Energy of the Inhibitor onto the Crystal Surfaces. In this study, the inhibitors were adsorbed on the Fe (110) surface through coordination bonds, wherein the central atom (N) of the inhibitors possesses unshared electron pairs. When an empty d orbital is present on the metal surface, a coordination bond is formed between the single pair electron of the polar group's central atom and the empty d orbital. The energy of two organic corrosion inhibitors interacting with a metal surface was also calculated according to the equation[47,48]

$$E_{binding} = E_{mol\text{-}Fe(110)} - (E_{mol} + E_{Fe(110)}) \quad (10)$$

Table 1. HOMO and LUMO Energies (eV), Ionization Energies (IEs), Electron Affinities (EAs), and $E_{LUMO\text{-}HOMO}$ Energy Gaps ($E_{L\text{-}H}$) for Inhibitors

inhibitor	LUMO	HOMO	IE	EA	$E_{L\text{-}H}$
GLU	−1.269	−5.521	5.521	1.269	4.252
PASP	−2.217	−5.942	5.942	2.217	3.725
PASP + GLU	−2.336	−5.759	5.759	2.336	3.423

where E_{mol} and $E_{Fe(110)}$ are the energies of the single organic molecule and Fe (110) surface, respectively, and $E_{mol\text{-}Fe(110)}$ is the total energy of the organo-Fe (110) complex. As shown in Table 2, negative $E_{binding}$ values were obtained in all groups, indicating that the attachment of both GLU and PASP on the Fe (110) surface was exothermic. The calculated $E_{binding}$ of PASP + GLU (−102.32 kJ/mol) is much more negative than

https://doi.org/10.1021/acsomega.3c05625
ACS Omega 2023, 8, 39709−39719

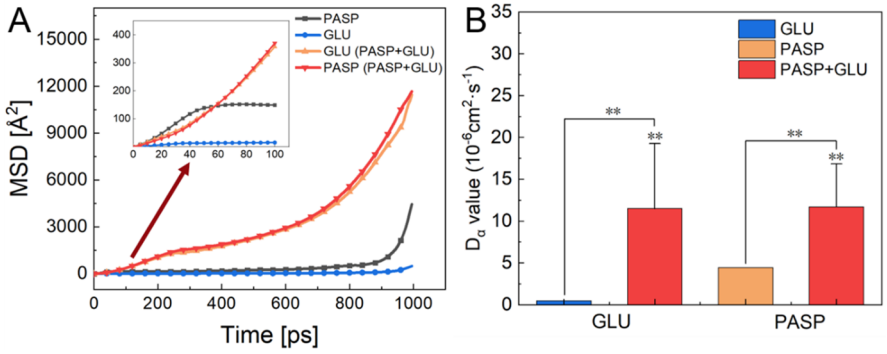

Figure 8. (A) MSD plots of PASP and GLU using the FFT-GGA function. (B) Diffusion coefficients of PASP and GLU molecules in different groups. The data were analyzed with an independent *t* test standard deviation, and the significance levels were expressed at $*p < 0.05$ and $**p < 0.01$.

Table 2. Binding Energies of Two Organic Molecules on Fe(110) ($E_{binding}$)

model	molecule	$E_{mol\text{-}Fe(110)}$ (kcal/mol)	$E_{binding}$ (kcal/mol)
1	GLU	−75.34	−39.35
2	PASP	−238.97	−73.92
3	PASP + GLU	−289.06	−102.32

that of individual PASP or GLU. Generally, a more negative $E_{binding}$ suggests a better adsorption performance. Thus, the adsorption performance of the combined corrosion inhibitors (PASP and GLU) is remarkably enhanced. These results were also consistent with the EIS data. Therefore, GLU could enhance the attachment of PASP on carbon steel with higher binding energy and thus improve the corrosion inhibition by forming a dense and stable protective layer (Figure 9).

3.6. Corrosion Inhibition Mechanism. According to the experimental results and theoretical calculations, the corrosion inhibition mechanism of PASP + GLU is illustrated in Figure 10. After adding PASP + GLU, GLU could bind with PASP via a donor−acceptor interaction between carboxyl groups and amino groups or adjacent carbon chains, accelerate the diffusion and attachment of PASP on a carbon steel surface, promote PASP forming a protective layer by inhibiting the access of corrosive medium, and thus enhance the corrosion inhibition of PASP for carbon steel. Meanwhile, PASP and GLU molecules could mutually fill in the vacancies produced in their individual adsorption, forming a more compact adsorbed inhibitor film to prevent carbon steel from attack of corrosive medium.

4. CONCLUSIONS

In this study, GLU was selected to enhance the corrosion inhibition of PASP on Q235 carbon steel, and their synergistic mechanism on corrosion inhibition was explored. GLU could promote PASP forming a dense and stable protective film on steel and thus improve the corrosion inhibition of PASP. The main mechanisms are as follows. (1) The interaction between GLU and PASP occurred at carboxyl groups and amino groups via donor−acceptor interactions. (2) GLU could accelerate the diffusion of PASP to the carbon steel surface with high diffusion coefficients. (3) The binding between PASP and the carbon steel surface improved greatly in the presence of GLU. Instead of developing new corrosion inhibitors, our study provides a new strategy to enhance existing corrosion inhibitors with glutamic acid, which would significantly reduce the cost of cooling water treatment and reduce adverse environmental impacts. Besides, we will focus on the roles of

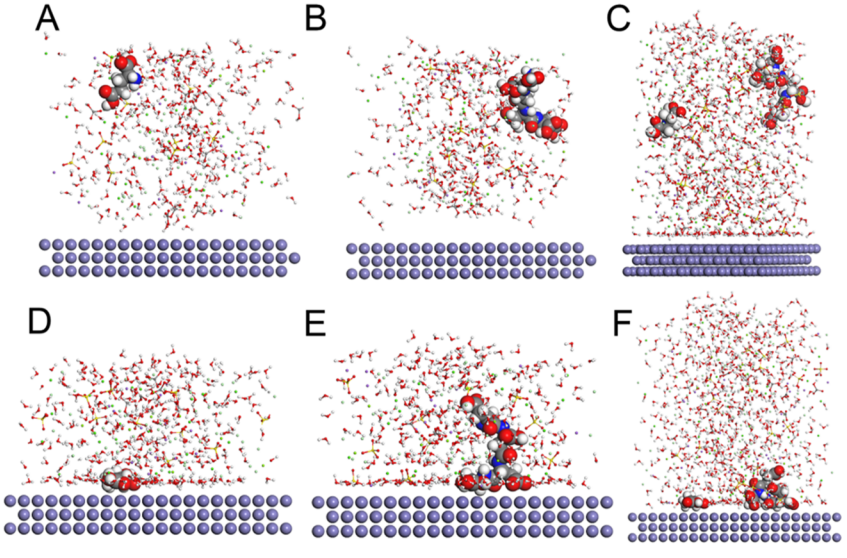

Figure 9. Attachment of organic molecules on metal surfaces in GLU (A, D), PSAP (B, E), and PASP + GLU groups (C, F).

https://doi.org/10.1021/acsomega.3c05625
ACS Omega 2023, 8, 39709−39719

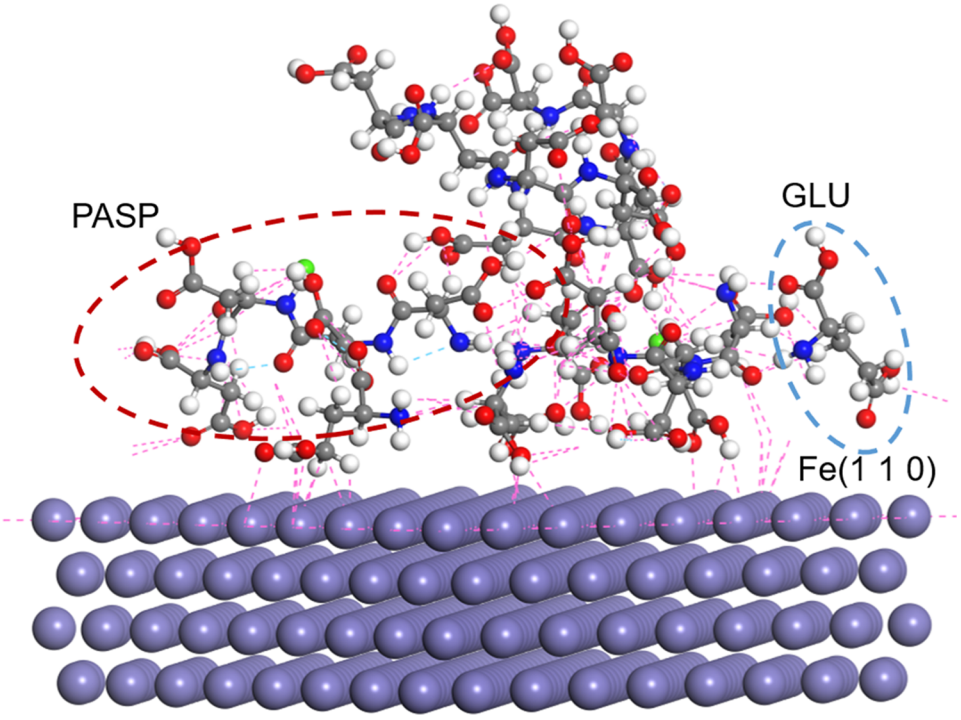

Figure 10. Interaction force between GLU and PASP on the Fe (110) surface at 303 K as obtained from MD simulations.

amino acids in mitigating microbiologically influenced corrosion in the future due to their great contribution to corrosion.

■ ASSOCIATED CONTENT

Supporting Information

The Supporting Information is available free of charge at https://pubs.acs.org/doi/10.1021/acsomega.3c05625.

Pretreatment of coupons before determining weight loss, SEM and AFM images, the constant phase element (Q), the two-dimensional structures of GLU and PASP, fitting parameters of EIS for Q235 carbon steel in four systems at different times, and electrochemical parameters of the potentiodynamic polarization curve of Q235 steel in different groups (PDF)

■ AUTHOR INFORMATION

Corresponding Author

Chao Song − *Shandong Key Laboratory of Water Pollution Control and Resource Reuse, School of Environmental Science and Engineering, Shandong University, Qingdao, Shandong 266237, People's Republic of China; Shandong Key Laboratory of Environmental Processes and Health, School of Environmental Science and Engineering, Shandong University, Qingdao, Shandong 266237, People's Republic of China;* orcid.org/0000-0001-9434-2973; Phone: +86 532 58630936; Email: songchao@sdu.edu.cn; Fax: +86 532 58630907

Authors

Shichu Gong − *Shandong Key Laboratory of Water Pollution Control and Resource Reuse, School of Environmental Science and Engineering, Shandong University, Qingdao, Shandong 266237, People's Republic of China; Shandong Key Laboratory of Environmental Processes and Health, School of Environmental Science and Engineering, Shandong University, Qingdao, Shandong 266237, People's Republic of China*

Yutong Li − *Shandong Key Laboratory of Water Pollution Control and Resource Reuse, School of Environmental Science and Engineering, Shandong University, Qingdao, Shandong 266237, People's Republic of China; Shandong Key Laboratory of Environmental Processes and Health, School of Environmental Science and Engineering, Shandong University, Qingdao, Shandong 266237, People's Republic of China*

Hongyi Li − *Shandong Key Laboratory of Water Pollution Control and Resource Reuse, School of Environmental Science and Engineering, Shandong University, Qingdao, Shandong 266237, People's Republic of China; Shandong Key Laboratory of Environmental Processes and Health, School of Environmental Science and Engineering, Shandong University, Qingdao, Shandong 266237, People's Republic of China*

Lin He − *Shandong Key Laboratory of Water Pollution Control and Resource Reuse, School of Environmental Science and Engineering, Shandong University, Qingdao, Shandong 266237, People's Republic of China; China Railway Fifth Survey and Design Institute Group CO., LTD., Beijing 12600, People's Republic of China*

Zhen Yan − *Shandong Key Laboratory of Water Pollution Control and Resource Reuse, School of Environmental Science and Engineering, Shandong University, Qingdao, Shandong 266237, People's Republic of China; Shandong Key Laboratory of Environmental Processes and Health, School of Environmental Science and Engineering, Shandong University, Qingdao, Shandong 266237, People's Republic of China;* orcid.org/0000-0002-6213-9054

Shuguang Wang − *Shandong Key Laboratory of Water Pollution Control and Resource Reuse, School of Environmental Science and Engineering, Shandong*

https://doi.org/10.1021/acsomega.3c05625
ACS Omega 2023, 8, 39709−39719

University, Qingdao, Shandong 266237, People's Republic of China; Shandong Key Laboratory of Environmental Processes and Health, School of Environmental Science and Engineering and Sino-French Research Institute for Ecology and Environment (ISFREE), School of Environmental Science and Engineering, Shandong University, Qingdao, Shandong 266237, People's Republic of China; WeiHai Research Institute of Industrial Technology of Shandong University, Weihai 264209, People's Republic of China; orcid.org/0000-0002-9381-1771

Xiaomin Sun − *Environment Research Institute, Shandong University, Qingdao 266237, People's Republic of China*

Complete contact information is available at: https://pubs.acs.org/10.1021/acsomega.3c05625

Author Contributions

S.G.: methodology, investigation, formal analysis, writing - original draft, writing - review and editing. Y.L.: methodology, formal analysis. H.L.: methodology, investigation, formal analysis. Z.Y.: formal analysis, writing - review and editing. S.W.: resources, funding acquisition, writing - review and editing. X.S.: formal analysis, writing - review and editing. C.S.: conceptualization, methodology, supervision, resources, formal analysis, writing - original draft, writing - review and editing

Notes

The authors declare no competing financial interest.

■ ACKNOWLEDGMENTS

This research was supported by the National Natural Science Foundation of China (U20A20146 and 22378232), the Young Scholars Program of Shandong University, and the Taishan Scholars Project of Shandong Province (No. tstp20230604). We thank Haiyan Yu, Xiaomin Zhao, Yuyu Guo, and Sen Wang from Core Facilities for Life and Environmental Sciences of SKLMT (State Key Laboratory of Microbial Technology, Shandong University) for assistance with SEM microscopy imaging.

■ REFERENCES

(1) A M Peer, R.; T Sanders, K. Characterizing cooling water source and usage patterns across US thermoelectric power plants: a comprehensive assessment of self-reported cooling water data. *Environ. Res. Lett.* **2016**, *11* (12), 124030.

(2) Popoola, L. T. Corrosion problems during oil and gas production and its mitigation. *Int. J. Ind. Chem.* **2013**, *4* (1), 1.

(3) Perez, T. E. Corrosion in the Oil and Gas Industry: An Increasing Challenge for Materials. *Jom* **2013**, *65* (8), 1033−1042.

(4) Sanders, K. T. Critical review: Uncharted waters? The future of the electricity-water nexus. *Environ. Sci. Technol.* **2015**, *49* (1), 51−66.

(5) Finšgar, M.; Jackson, J. Application of corrosion inhibitors for steels in acidic media for the oil and gas industry: A review. *Corros. Sci.* **2014**, *86*, 17−41.

(6) Chen, Y.; Xie, X. G.; Ren, C. G.; Dai, C. C. Degradation of N-heterocyclic indole by a novel endophytic fungus Phomopsis liquidambari. *Bioresour. Technol.* **2013**, *129*, 568−574.

(7) Padoley, K. V.; Mudliar, S. N.; Pandey, R. A. Heterocyclic nitrogenous pollutants in the environment and their treatment options-an overview. *Bioresour. Technol.* **2008**, *99* (10), 4029−4043.

(8) Zhu, H.; Han, Y.; Ma, W.; Han, H.; Ma, W. Removal of selected nitrogenous heterocyclic compounds in biologically pretreated coal gasification wastewater (BPCGW) using the catalytic ozonation process combined with the two-stage membrane bioreactor (MBR). *Bioresour. Technol.* **2017**, *245*, 786−793.

(9) Adelnia, H.; Sirous, F.; Blakey, I.; Ta, H. T. Metal ion chelation of poly(aspartic acid): From scale inhibition to therapeutic potentials. *Int. J. Biol. Macromol.* **2023**, *229*, 974−993.

(10) Zeino, A.; Abdulazeez, I.; Khaled, M.; Jawich, M. W.; Obot, I. B. Mechanistic study of polyaspartic acid (PASP) as eco-friendly corrosion inhibitor on mild steel in 3% NaCl aerated solution. *J. Mol. Liq.* **2018**, *250*, 50−62.

(11) Jiang, M.; Chen, L.-Y.; Zou, Q.; Xiong, S.; Fu, P.; Gai, J.-G. Zwitterionic and hydrophilic polyelectrolyte/metal ion anti-fouling layersviacovalent and coordination bonds for reverse osmosis membranes. *Mater. Chem. Front.* **2021**, *5* (11), 4202−4213.

(12) Kadhim, M. M.; Alabboodi, K. O.; Hachim, S. K.; Abdullaha, S. A.; Taban, T. Z.; Rheima, A. M. Analysis of the protection of copper corrosion by using amino acid inhibitors. *J. Mol. Model.* **2023**, *29* (1), 27.

(13) Naundorf, T.; Seddig, T.; Ruf, E.; Ballentin, L.; Kipphardt, H.; Maison, W. Alkali salts of amino acids as alkaline additives for neutralization of acidic corrosion inhibitors. *Amino Acids* **2023**, *55*, 665.

(14) Xu, J.; Jia, R.; Yang, D.; Sun, C.; Gu, T. Effects of d-Phenylalanine as a biocide enhancer of THPS against the microbiologically influenced corrosion of C1018 carbon steel. *J. Mater. Sci. Technol.* **2019**, *35* (1), 109−117.

(15) Dragčević, Đ.; Bišćan, J. Surface potential of *β*-alanine at the electrolyte/air and artificial seawater/air interface. *Colloids Surf., A* **2003**, *223* (1−3), 35−43.

(16) Fawzy, A.; Al Bahir, A.; Alqarni, N.; Toghan, A.; Khider, M.; Ibrahim, I. M.; Abulreesh, H. H.; Elbanna, K. Evaluation of synthesized biosurfactants as promising corrosion inhibitors and alternative antibacterial and antidermatophytes agents. *Sci. Rep.* **2023**, *13* (1), 2585.

(17) Largo, L.; Redondo, P.; Rayón, V. M.; Largo, A.; Barrientos, C. The reaction between NH3+and CH3COOH: a possible process for the formation of glycine precursors in the interstellar medium. *Astron. Astrophys.* **2010**, *516*, A79.

(18) Li, C.; Zhang, C.; Zhang, W. The inhibitory effects of four inhibitors on the solution adsorption of CaCO3 on Fe3O4 and Fe2O3 surfaces. *Sci. Rep.* **2019**, *9* (1), 13724.

(19) Zhang, B.; He, C.; Wang, C.; Sun, P.; Li, F.; Lin, Y. Synergistic corrosion inhibition of environment-friendly inhibitors on the corrosion of carbon steel in soft water. *Corros. Sci.* **2015**, *94*, 6−20.

(20) Berdimurodov, E.; Kholikov, A.; Akbarov, K.; Guo, L. Experimental and theoretical assessment of new and eco-friendly thioglycoluril derivative as an effective corrosion inhibitor of St2 steel in the aggressive hydrochloric acid with sulfate ions. *J. Mol. Liq.* **2021**, *335*, 116168.

(21) Kolodkin-Gal, I.; Romero, D.; Cao, S.; Clardy, J.; Kolter, R.; Losick, R. D-amino acids trigger biofilm disassembly. *Science* **2010**, *328* (5978), 627−629.

(22) Obot, I. B.; Macdonald, D. D.; Gasem, Z. M. Density functional theory (DFT) as a powerful tool for designing new organic corrosion inhibitors. Part 1: An overview. *Corros. Sci.* **2015**, *99*, 1−30.

(23) Ramezanzadeh, M.; Bahlakeh, G.; Sanaei, Z.; Ramezanzadeh, B. Corrosion inhibition of mild steel in 1 M HCl solution by ethanolic extract of eco-friendly Mangifera indica (mango) leaves: Electrochemical, molecular dynamics, Monte Carlo and ab initio study. *Appl. Surf. Sci.* **2019**, *463*, 1058−1077.

(24) Saha, S. K.; Ghosh, P.; Hens, A.; Murmu, N. C.; Banerjee, P. Density functional theory and molecular dynamics simulation study on corrosion inhibition performance of mild steel by mercaptoquinoline Schiff base corrosion inhibitor. *Phys. E* **2015**, *66*, 332−341.

(25) Saha, S. K.; Murmu, M.; Murmu, N. C.; Banerjee, P. Evaluating electronic structure of quinazolinone and pyrimidinone molecules for its corrosion inhibition effectiveness on target specific mild steel in the acidic medium: A combined DFT and MD simulation study. *J. Mol. Liq.* **2016**, *224*, 629−638.

(26) Al-Mobarak, N. A.; Khaled, K. F.; Hamed, M. N. H.; Abdel-Azim, K. M. Employing electrochemical frequency modulation for

studying corrosion and corrosion inhibition of copper in sodium chloride solutions. *Arabian J. Chem.* **2011**, *4* (2), 185−193.
(27) Delley, B. Hardness conserving semilocal pseudopotentials. *Phys. Rev. B* **2002**, *66* (15), 155125.
(28) Perdew, J. P. Generalized Gradient Approximation Made Simple. *Phys. Rev. Lett.* **1996**, *78*, 1396.
(29) Tkatchenko, A.; Scheffler, M. Accurate molecular van der Waals interactions from ground-state electron density and free-atom reference data. *Phys. Rev. Lett.t* **2009**, *102* (7), 073005.
(30) Qian, B.; Wang, J.; Zheng, M.; Hou, B. Synergistic effect of polyaspartic acid and iodide ion on corrosion inhibition of mild steel in H2SO4. *Corros. Sci.* **2013**, *75*, 184−192.
(31) Aramaki, K.; Hackerman, N. Inhibition mechanism of medium-sized poly-methyleneimine. *J. Electrochem. Soc.* **1969**, *116* (5), 568.
(32) El-Mokadem, T. H.; Hashem, A. I.; Abd El-Sattar, N. E. A.; Dawood, E. A.; Abdelshafi, N. S. Green synthesis, electrochemical, DFT studies and MD simulation of novel synthesized thiourea derivatives on carbon steel corrosion inhibition in 1.0 M HCl. *J. Mol. Struct.* **2023**, *1274*, 134567.
(33) Abrishami, S.; Naderi, R.; Ramezanzadeh, B. Fabrication and characterization of zinc acetylacetonate/Urtica Dioica leaves extract complex as an effective organic/inorganic hybrid corrosion inhibitive pigment for mild steel protection in chloride solution. *Appl. Surf. Sci.* **2018**, *457*, 487−496.
(34) Tian, H.; Li, W.; Hou, B.; Wang, D. Insights into corrosion inhibition behavior of multi-active compounds for X65 pipeline steel in acidic oilfield formation water. *Corros. Sci.* **2017**, *117*, 43−58.
(35) Li, S.; Qu, Q.; Li, L.; Xia, K.; Li, Y.; Zhu, T. Bacillus cereus s-EPS as a dual bio-functional corrosion and scale inhibitor in artificial seawater. *Water. Res.* **2019**, *166*, 115094.
(36) Yang, X.; Shao, J.; Liu, Z.; Zhang, D.; Cui, L.; Du, C.; Li, X. Stress-assisted microbiologically influenced corrosion mechanism of 2205 duplex stainless steel caused by sulfate-reducing bacteria. *Corros. Sci.* **2020**, *173*, 108746.
(37) Chen, S.; Deng, H.; Zhao, Y.; Lu, S.; Zhao, Y.; Cheng, X.; Liu, G.; Dou, W.; Chen, J. The effects of Methanococcus maripaludis on the corrosion behavior of EH40 steel in seawater. *Bioelectrochemistry* **2021**, *140*, 107824.
(38) Ghods, P.; Isgor, O. B.; McRae, G.; Miller, T. The effect of concrete pore solution composition on the quality of passive oxide films on black steel reinforcement. *Cem. Concr. Compos* **2009**, *31* (1), 2−11.
(39) AU Zhu, Z.; Liang, X.; Zhang, R.; AF Zhu, Z.; Liang, X.; Zhang, R. Determination of the dissociation constants of polyaspartic acid. Chin. J. *Chin J. Anal. Chem.* **2005**, *33* (12), 1722−1724.
(40) Asadi, N.; Ramezanzadeh, M.; Bahlakeh, G.; Ramezanzadeh, B. Utilizing Lemon Balm extract as an effective green corrosion inhibitor for mild steel in 1M HCl solution: A detailed experimental, molecular dynamics, Monte Carlo and quantum mechanics study. *J. Taiwan Inst. Chem. Eng.* **2019**, *95*, 252−272.
(41) Khaled, K. F. Studies of iron corrosion inhibition using chemical, electrochemical and computer simulation techniques. *Electrochimi. Acta.* **2010**, *55* (22), 6523−6532.
(42) Musa, A. Y.; Jalgham, R. T. T.; Mohamad, A. B. Molecular dynamic and quantum chemical calculations for phthalazine derivatives as corrosion inhibitors of mild steel in 1M HCl. *Corros. Sci.* **2012**, *56*, 176−183.
(43) Zhang, J.; Qiao, G.; Hu, S.; Yan, Y.; Ren, Z.; Yu, L. Theoretical evaluation of corrosion inhibition performance of imidazoline compounds with different hydrophilic groups. *Corros. Sci.* **2011**, *53* (1), 147−152.
(44) Chen, X.; Chen, Y.; Cui, J.; Li, Y.; Liang, Y.; Cao, G. Molecular dynamics simulation and DFT calculation of "green" scale and corrosion inhibitor. *Comput. Mater. Sci.* **2021**, *188*, 110229.
(45) Kokalj, A.; Lozinšek, M.; Kapun, B.; Taheri, P.; Neupane, S.; Losada-Pérez, P.; Xie, C.; Stavber, S.; Crespo, D.; Renner, F. U. Simplistic correlations between molecular electronic properties and inhibition efficiencies: Do they really exist? *Corros. Sci.* **2021**, *179*, 108856.
(46) Morales-Gil, P.; Walczak, M. S.; Cottis, R. A.; Romero, J. M.; Lindsay, R. Corrosion inhibitor binding in an acidic medium: Interaction of 2-mercaptobenizmidazole with carbon-steel in hydrochloric acid. *Corros. Sci.* **2014**, *85*, 109−114.
(47) Shi, W.; Xu, W.; Cang, H.; Yan, X.; Shao, R.; Zhang, Y.; Xia, M. Design and synthesis of biodegradable antiscalant based on MD simulation of antiscale mechanism: A case of itaconic acid-epoxysuccinate copolymer. *Comput. Mater. Sci.* **2017**, *136*, 118−125.
(48) Zuo, Z.; Yang, W.; Zhang, K.; Chen, Y.; Li, M.; Zuo, Y.; Yin, X.; Liu, Y. Effect of scale inhibitors on the structure and morphology of CaCO3 crystal electrochemically deposited on TA1 alloy. *J. Colloid Interface Sci.* **2020**, *562*, 558−566.

https://doi.org/10.1021/acsomega.3c05625
ACS Omega 2023, 8, 39709−39719